AAPS PharmSciTech (2023) 24:222
https://doi.org/10.1208/s12249-023-02683-9

RESEARCH ARTICLE

Nanohybrid Based on (Mn, Zn) Ferrite Nanoparticles Functionalized With Chitosan and Sodium Alginate for Loading of Curcumin Against Human Breast Cancer Cells

Fatemeh Ahmadi[1,2] · Majid Saeedi[2] · Jafar Akbari[2] · Mohammad Seyedabadi[3] · Pedram Ebrahimnejad[2,4] · Katayoun Morteza-Semnani[5] · Shahram Ghasemi[6] · Monire Moalem-Banhangi[6] · Amirhossein Babaei[1,2] · Seyyed Mohammad Hassan Hashemi[7] · Kofi Asare-Addo[8] · Ali Nokhodchi[9,10]

Received: 1 July 2023 / Accepted: 18 October 2023 / Published online: 7 November 2023

Abstract

This study reports on the synthesis of $Mn_{1-x}Zn_xFe_2O_4$ (Mn, Zn ferrite) magnetic nanoparticles (MNPs) as drug delivery carriers for effective therapeutic outcomes. The MNPs were prepared using the coprecipitation method, and their magnetic properties were investigated based on their composition. Among the compositions tested, $Mn_{0.8}Zn_{0.2}Fe_2O_4$ MNPs exhibited superparamagnetic properties with a saturation magnetization moment of 34.6 emu/g at room temperature (25°C). To enhance the water solubility of curcumin (Cur), known for its hydrophobic nature, it was successfully loaded onto alginate (Alg)/chitosan (Chit)@$Mn_{0.8}Zn_{0.2}Fe_2O_4$ nanoparticles (NPs). The nanocomposite was characterized by field emission scanning electron microscopy (FE-SEM) which revealed a particle size of approximately 20 nm. The crystalline structure of the NPs was analyzed using X-ray diffraction, while Fourier-transform infrared (FTIR), energy-dispersive X-ray, and map analysis techniques were employed for further characterization. In terms of drug release, there was an initial burst release of Cur (around 18%) within the first hour, followed by a slower release (approximately 61%) over the next 36 h. The anti-tumor properties of the Cur-loaded NPs were evaluated using the Methyl Thiazol Tetrazolium (MTT) assay and quantitative real-time polymerase chain reaction. The MTT assay confirmed a higher cytotoxic effect of Cur-loaded Alg/Chit@$Mn_{0.8}Zn_{0.2}Fe_2O_4$ NPs on the MCF-7 breast cancer cell line compared to free Cur, highlighting the significance of incorporating Cur into nano-sized carrier systems.

Keywords alginate · breast cancer · chitosan · curcumin · drug release · magnetic nanoparticles

✉ Majid Saeedi
m.saeedi@mazums.ac.ir

✉ Ali Nokhodchi
A.Nokhodchi@sussex.ac.uk; AliNokhodchi@lupin.com

1 Student Research Committee, Faculty of Pharmacy, Mazandaran University of Medical Sciences, Sari, Iran

2 Department of Pharmaceutics, Faculty of Pharmacy, Mazandaran University of Medical Sciences, Sari, Iran

3 Department of Toxicology and Pharmacology, Faculty of Pharmacy, Mazandaran University of Medical Sciences, Sari, Iran

4 Pharmaceutical Sciences Research Center, Hemoglobinopathy Institute, Mazandaran University of Medical Sciences, Sari, Iran

5 Department of Medicinal Chemistry, Faculty of Pharmacy, Mazandaran University of Medical Sciences, Sari, Iran

6 Faculty of Chemistry, University of Mazandaran, Babolsar, Iran

7 Department of Pharmaceutics, Faculty of Pharmacy, Hormozgan University of Medical Sciences, Bandar Abaas, Iran

8 Department of Pharmacy, University of Huddersfield, Huddersfield HD1 3DH, UK

9 Pharmaceutical Research Laboratory, School of Life Sciences, University of Sussex, Brighton, UK

10 Lupin Pharmaceutical Research Center, Coral Springs, Florida, USA

Introduction

Nanomaterials have shown considerable potential to cure a wide range of diseases. Among these nanomaterials, magnetite nanoparticles (MNPs) have attracted much attention because of their unique properties [1, 2]. At present, magnetic oxide complexes containing iron ions have attracted significant interest owing to the intricate interplay between their functional attributes and chemical composition [3, 4]. The presence of optimal magnetic and electrical properties [5] as well as microwave characteristics [6] renders these iron oxides highly suitable for various practical applications.

Magnetic oxide complexes have been used in several fields such as catalysis, drug delivery, protein separation, magnetic resonance imaging (MRI), and magnetic sensors [7–9]. Some studies have revealed the positive effects of doping iron oxide NPs with B_2O_3, Co, or Zn ions on magnetic parameters, including permeability and saturation magnetization [10]. Because of their superparamagnetic activity at room temperature, $ZnFe_2O_4$ NPs are attracting much attention in the biomedical sector [11]. $MnFe_2O_4$ NPs are receiving intensive attention for their significant inherent biocompatibility due to the doping of Mn^{2+} ions, higher transition temperature, tunable magnetic response, and considerable chemical stability at room temperature [12, 13].

Mn-Zn ferrite have distinctive physical and chemical properties such as low core loss; high magnetic permeability; and thermal, mechanical, and magnetic properties [14, 15]. The chemical and physical properties of magnetic ferrite NPs mainly rely on their preparation conditions and techniques used. Numerous methods have therefore been used in the production of NPs of Zn–Mn ferrite. These include high-energy ball milling [16], co-precipitation [17], sol–gel [18], microemulsion [19], and the hydrothermal technique [20]. The co-precipitation technique seems to be the utmost promising technique because of its high productivity and simplicity of use [21].

The ferrite NP surfaces have also been decorated with biocompatible/biodegradable polymers to improve their surface properties. Several reports have suggested the use of surface coatings such as chitosan (Chit) [22], alginate (Alg) [23], polyethylene glycol (PEG) [24], and dextran [25] for the MNPs.

Among various marine biomaterials, Chit has attracted great attention because of its biodegradable, biocompatible, and bioactive properties. Chit is widely used in medical and pharmaceutical applications, including artificial matrices for drug delivery [26], tissue engineering [27], wound dressing [28], and anti-bacterial coatings [29]. Metal oxide NPs have also been incorporated into various Chit matrix forms such as films or gels.

Alg is a naturally linear polysaccharide that has attracted attention in the progress of advanced drug delivery systems based on electrostatic interactions [30, 31]. The most significant properties of this polysaccharide are biocompatibility, nontoxicity, biodegradability, water solubility, and accessibility of carboxyl and hydroxyl functionalities for chemical modification [32, 33].

Recent research implies that curcumin (Cur) has gained considerable attention due to its multiple pharmacological effects, such as an anti-oxidant [34], anti-inflammatory [35], anti-microbial [36], and has a wide spectrum of actions against tumors [37]. Many researchers have demonstrated that Cur modulates cancer cell growth by the interference with multiple cellular signaling pathways, including mitochondrial pathways, caspase activation, tumor suppressor, cell proliferation, and survival [38–40]. Despite the excellent biological properties of Cur, the administration of Cur is restricted due to its low bioavailability, instability, low aqueous solubility, and thus poor absorption. Several methods have been used to overcome the low aqueous solubility of Cur through encapsulation in liposomes [41], dendrimers [42], cyclodextrin [43], and hydrogels [44]. It has also been reported that encapsulated Cur in nanoformulations is effectively protected against degradation and assists in its delivery to target cells [45, 46].

Based on the above information, to the best of our knowledge, there have been a few reports on the examination of the usage of rare-earth-doped Mn–Zn ferrites on cancer cells. The electrical, microwave, and magnetic properties of ferrite spinels are noteworthy for applications as functional materials in high-frequency and biomedical uses. High residual magnetization and low coercive force (optimal magnetic properties) permit the application of spinels for targeted drug delivery in humans through a magnetic field. The current work aimed to develop curcumin (Cur)-loaded alginate/chitosan@$Mn_{1-x}Zn_x$-Fe_2O_4 nanoparticles (NPs) using the nanoprecipitation method. In this study, we opted for $Mn_{1-x}Zn_xFe_2O_4$ nanocarriers due to their simplicity in preparation, resulting in small-sized particles, and possessing the requisite magnetization to enable responsiveness to an external magnetic field. Subsequently, a comprehensive investigation was conducted into the physicochemical characteristics and *in vitro* efficacy of Cur-loaded alginate/chitosan@$Mn_{0.8}Zn_{0.2}Fe_2O_4$ NPs. The performance of these NPs and a curcumin solution were then evaluated against MCF-7 human breast cancer cell lines to determine its effectiveness.

Materials and Methods

Materials

Low molecular weight (50,000–190,000 Da) chitosan (Chit), alginate (Alg), ethylene glycol (EG), citric acid, sodium

dodecyl sulfate (SDS), and Na_2SO_4 were purchased from Fluka (Switzerland). Curcumin (Cur) powder was obtained from Merck Company, Darmstadt, Germany. Manganese nitrate ($Mn(NO_3)_4H_2O$), zinc nitrate (($Zn(NO_3)_2.6H_2O$), ferric chloride ($FeCl_3$ anhydrous), 3-[4, 5-2-yl]-2,5-diphenyl-tetrazolium bromide (MTT) assay, Dulbecco's modified eagle medium (DMEM), Roswell Park Memorial Institute (RPMI) 1640 medium, fetal bovine serum (FBS), penicillin/streptomycin (P/S), l-glutamine, and trypsin/EDTA were all obtained from Sigma-Aldrich (Germany). The human breast cancer (MCF-7) cell lines were purchased from the Pasteur Institute, Tehran, Iran.

Preparation of Cur-Loaded Alg/Chit@(Mn, Zn) Ferrite NPs

Synthesis of (Mn, Zn) Ferrite NPs

$(Mn_{1-x}Zn_x)$ Fe_2O_4 NPs were fabricated using a simple co-precipitation technique with an x value from 0.2 to 0.8. For the co-precipitation method, 1.36 g of ferric chloride ($FeCl_3$ anhydrous), 0.97–0.33 g of manganese nitrate ($Mn(NO_3)_2.4H_2O$), and 0.39–1.16 g of zinc nitrate (($Zn(NO_3)_2.6H_2O$)) was dissolved in 50 mL of de-ionized water. Five-milliliter hydrochloric acid (0.2 M) and 10 mL EG were then added slowly to the solution under stirring conditions (500 rpm on a stirring plate at room temperature (25°C) for 30 min). After that, in a three round-neck bottom flask (250 mL) equipped with a magnetic stirring bar, 0.54 g SDS and 3 g sodium hydroxide were dissolved in distilled water at about 80°C. The former solution was poured slowly into the flask under stirring (700 rpm), which was continued for 1 h under a N_2 atmosphere at 80°C. The precipitate was washed three times with 120 mL of de-ionized water and absolute ethanol and then centrifuged for 10 min at 8000 rpm. To induce the surface modification of (Mn, Zn) ferrite NPs, the mixture was modified by adding 0.05 M citric acid. This mixture was stirred (500 rpm) together for 1 h under N_2 at 85°C. At the end of the reaction, the resulting mixture was washed three times with 120 mL de-ionized water and then centrifuged for 20 min at 14,000 rpm.

Synthesis of Cur-Loaded Alg/Chit@(Mn, Zn)Ferrite NPs

For the synthesis of Cur incorporated Alg/Chit@ $Mn_{0.8}Zn_{0.2}Fe_2O_4$ NPs**,** 50 mg of Chit was dissolved in 50 mL 1% acetic acid with the pH adjusted to 4.9 by use of a 1 M sodium hydroxide solution. Cur powder (5 mg) was dissolved in 5 mL absolute ethanol and added to the Chit solution at a stirring speed of 700 rpm. The Cur-loaded Chit solutions were introduced into a modified $Mn_{0.8}Zn_{0.2}Fe_2O_4$ NP mixture under stirring (700 rpm). Twenty-five-milliliter Alg (1 mg/mL) solution was then added to the mixed solution and the pH of the suspension was adjusted to 4.6 by the use of a 0.5 M hydrochloric acid solution. The Alg was injected slowly into this solution. Finally, the obtained NPs were washed three times with 120 mL of de-ionized water and ethanol, respectively, and then centrifuged for 20 min at 14,000 rpm. Finally, the product was dried at room temperature (25°C) for 24 h.

Characterization

Dynamic light scattering (DLS) is a well-established and non-invasive technique for determining the size distribution and size of small particles in the submicron region. DLS via a Zetasizer Nano ZS system (Malvern Instruments Worcestershire: UK) with an angle of 90° at 25°C was applied to measure the diameter of the NPs. Laser Doppler electrophoresis was applied to determine the zeta potential of the NPs. The final concentration of the sample was 0.05 ppm.

Loading Capacity

The amount of loaded Cur was measured by high-performance liquid chromatography (HPLC) analysis (Knauer; Smartline, Berlin, Germany). The Cur-loaded Alg/Chit@$Mn_{0.8}Zn_{0.2}Fe_2O_4$ solution in the "Synthesis of (Mn, Zn) Ferrite NPs" section was centrifuged, and the supernatant was decanted. Air-dried NPs (1 mg) were dissolved in ethanol 70% (1 mL), and the Cur-loaded nanocomposite was extracted using ethanol and acetonitrile. The mobile phase of the HPLC was a mixture of water, ethanol, and acetonitrile in a ratio of 30:30:40 (v/v), respectively. Eurospher 100-5 C18 5 µm, 4.6/250 mm was used as the column (Knauer, Berlin, Germany). The ultraviolet (UV) detector at a wavelength of 428 nm was used to detect the eluent, and the mobile phase had a flow rate of 1 mL/min. The EZChrom software was used to calculate the area under the peaks. The amount of Cur was calculated from the standard calibration curve derived from a range of Cur concentration of 2–50 µg mL^{-1}. Cur loading capacity of NPs was measured using the equation below:

$$Drug\ loading\ (\%) = Total\ amount\ of\ Cur\ in\ nanocomposite / Total\ weight\ of\ nanocomposite \times 100$$

Morphology

The morphologies (e.g., particle size and shape) of the samples were studied by a field-emission scanning electron microscope (FE-SEM) (Mira3, Tescan) equipped with an energy-dispersive X-ray (EDX) spectrometry and dynamic light scattering (DLS). In the FE-SEM analysis, the nanocomposite was scanned at 15 kV and had a working distance of 10.46 mm. To avoid charge buildup on the product

surface, it was covered with conductive metallic compounds, in this case, gold.

Fourier-Transform Infrared Analysis

A Cary 630 Fourier-transform infrared (FTIR) spectrophotometer (Agilent Technologies Inc., CA, USA) was used to identify the structural information of the starting materials (e.g., Cur, Alg, Chit) and Cur-loaded MNPs. The spectra were recorded between 400 and 4000 cm^{-1}.

X-ray Diffraction Analysis

The crystalline structure of Cur-loaded Alg/Chit@$Mn_{1-x}Zn_xFe_2O_4$ NPs was evaluated using X-ray diffraction (PHILIPS-PW1730; Netherland) (40 kV; 30 mA) at 2θ of between 10° and 80°. The samples were exposed to Cu Kα radiation ($\lambda = 1.5406$ A°) and scanned from 10 to 80° at 2θ with a step time equal to 1 s and a step size of 0.050°.

Vibrating-Sample Magnetometer Analysis

The magnetic moment of compounds as a function of the applied magnetic field was registered as a vibrating-sample magnetometer (VSM). The samples were placed in a gel capsule and then air dried. To prevent movements during the measurement, the samples were clamped using a sample holder. The maximum applied field was deemed to be about 2 T in a 10-mm air gap. Magnetization properties of the NPs were investigated with a VSM (MDKB, Kashan, Iran) at room temperature (25°C).

In Vitro Release Study

The *in vitro* release study is one of the important tests used to evaluate and assess the efficacy, safety, and quality of nanocomposite-based drug delivery systems [47, 48]. The dialysis bag (cutoff = 12–14 KD) method was used for the *in vitro* release study. Before starting the process, the dialysis bag was pre-treated/soaked in double-distilled water and kept overnight. The pre-treated dialysis bag was individually filled with 5 mg of samples (pure Cur and Cur-loaded Alg/Chit@$Mn_{0.8}Zn_{0.2}Fe_2O_4$). The bag was then tied at both ends and placed in 150 mL of dissolution media at 37°C. At time intervals of 0, 1, 3, 5, 7, 9, 11, 24, and 36 h, the dissolution medium was centrifuged at 14,000 rpm for 15 min. The released Cur was dissolved in absolute ethanol (2 mL), and the absorbance was determined via a UV spectrophotometer (SQ4802; UNICO, Dayton, NJ, USA) at $\lambda = 428$ nm. The *in vitro* release data was calculated based on the following equation:

$$Release\ (\%) = C_t / C_0 \times 100$$

where C_t indicates the released Cur concentration at the time t and C_0 is the total value of Cur-loaded in Alg/Chit@$Mn_{0.8}Zn_{0.2}Fe_2O_4$ NPs.

Cell Culture Examination

The MCF-7 cells were cultured in a DMEM-high glucose growth medium containing 10% of FBS and 1% of P/S. The cells were then incubated 5 h with 5% CO_2 at 37°C.

Cell Viability Assay (IC_{50})

The MTT assay was used to examine the Cur, nanocarrier, and nanocomposite's efficacy on the MCF-7 cells. The cancer cell was plated in a 96-well cell (1 × 105 cells/mL) at 200 µL and then incubated at 37°C with 5% CO_2 for 24 h. The cells were treated with various concentrations (15.62–250 µg/mL) of Cur, Alg/Chit@$Mn_{0.8}Zn_{0.2}Fe_2O_4$, and Cur-loaded Alg/Chit@$Mn_{0.8}Zn_{0.2}Fe_2O_4$. After 48 h of the incubation period, 20 µL of the MTT was incorporated into each well. After an incubation period of 4 h, 100 µL of DMSO was poured into each well to dissolve the blue formazan precipitate. Absorbance was subsequently measured at 570 nm by a microplate reader. The IC_{50} values were measured from the concentrations of Cur and Cur-loaded synthesized NPs, which prevent 50% of cell growth. The experimentations were performed in triplicate. The average absorbance was applied to measure the average cell viability by employing the following equation:

$$\%\ Cell\ viability = Average\ absorbance\ of\ treated\ sample / Average\ absorbance\ of\ control \times 100$$

The primary objective of this research was to explore and analyze the impact of various key parameters on the synthesis of nanomagnetic particles, specifically designed for drug delivery applications. In pursuit of this goal, the study focused primarily on the MTT assay as a crucial indicator of cell viability and compatibility with the produced nanomagnetic particles which have been the case in other studies [49–52]. However, it is worth acknowledging that the vast landscape of nanoparticle research offers a multitude of characterization and assessment techniques. Notably, some researchers have suggested the inclusion of cytotoxicity assays among other tests [53–55].

Statistical Analysis

One-way ANOVA was applied to examine the statistically significant differences between the groups. The data were

shown as mean ± SD. *P*-values < 0.05 were measured as being significant throughout the studies.

Results and Discussions

Characterization

DLS is an effective tool used to measure the size of NPs in an aqueous solution or suspension. The nanoparticles (NPs) were sonicated at room temperature (25°C). This resulted in average hydrodynamic diameters of 66.5 nm for (Mn, Zn) ferrite, 111.7 nm for Cur-loaded chitosan@(Mn, Zn) ferrite, and 122.4 nm for the Cur-loaded alginate/chitosan@(Mn, Zn) ferrite NPs (Table I). This methodology is very different from the imaging of dried compounds and is sensitive to dynamic aggregation and agglomeration of the particles in solution [56]. It is important to note that the different sizes of the samples in aqueous solutions and dry compounds can be caused by the Brownian motion of the particles in the aqueous solution [57]. The DLS histogram of Cur-loaded Alg/Chit@$Mn_{0.8}Zn_{0.2}Fe_2O_4$ NPs depicts that the NP size was in the range of 50–250 nm, with an average size distribution of 122.4 ± 4.10 nm (Fig. 1). It is important to also note that the surface charge can impact the NP distribution stability. NPs with high amounts of zeta potential in the range of 20 to 40 mV could be an indication of good nanoparticle stability and a reduction in the likelihood of an increase in the particle size or aggregation of nanoparticles occurring in the system. The surface charge of nanoparticles is also a vital factor for NPs to interact with oppositely charged cell membranes or make aggregates in blood flow. The blood cells and plasma commonly display a negative charge. NPs with a negative surface charge can reduce undesirable interactions with blood cells [58]. The zeta potential values of coated and non-coated/naked MNP suspensions are shown in Table I. The presence of Chit-Cur on MNPs creates positively charged amino groups (NH_3^+) (zeta potential = +46.5) appropriate to ionic interactions with negatively charged Alg. The negative charge on the Alg/Chit-Cur@(Mn, Zn) ferrite NPs comes from the carboxyl groups present on the surface of the Alg. It can be concluded that the variation in surface charge is mainly because of the difference in the functional groups on the surface of the NPs [59]. These values are an indication of the good colloidal stability of NPs.

Loading Capacity

The drug loading capacity of the NPs carrier is a significant parameter for therapeutic applications. To estimate the drug-loading potential of NPs, Cur, with a large spectrum of biological activities, was selected. Cur was chosen as an anti-tumor model drug to evaluate the uptake of the drug by Alg/Chit@$Mn_{0.8}Zn_{0.2}Fe_2O_4$ NPs as a nanocarrier. The drug loading percentages of Cur were validated using HPLC on the Cur-loaded Alg/Chit@$Mn_{0.8}Zn_{0.2}Fe_2O_4$ NP mixture in ethanol 70%. It must be mentioned that the concentration of Cur was calculated using the standard curve obtained from a series of standard solutions of Cur in ethanolic solution (70%) as explained in the "Loading Capacity" section. The loading capacity for NP was found to be about 35%. Pazouki *et al*. reported that the loading capacity of Cur-loaded carboxymethyl Chit-Fe_3O_4 NPs was <5% [60]. In the current study, the higher Cur loading capacity may have resulted from the usage of citric acid as a modifier of MNPs. It can therefore be concluded that the incorporation of citrate-modified MNPs strengthened the binding to Chit-Cur.

FE-SEM Analysis

FE-SEM shows the morphology and size of the Cur-loaded Alg/Chit@$Mn_{0.8}Zn_{0.2}Fe_2O_4$ surface (Fig. 2a, b, c). FE-SEM study reveals that synthesized NPs are spherical and well dispersed. FE-SEM images in the higher magnification displayed that the diameters of NPs are around 20 nm. The elemental composition of the nanocomposite was also analyzed by EDX measurements (Fig. 2d). The EDX results confirmed the existence of Fe, Zn, Mn, N, C, and O elements. The element mapping image of Cur-incorporated Alg/Chit@$Mn_{0.8}Zn_{0.2}Fe_2O_4$ is displayed in Fig. 2e, which indicates the uniform distributions of Fe, Zn, Mn, N, C, and O throughout the nanocomposite.

FTIR Analysis

The FTIR spectra of Cur, Chit, Alg, and Cur-loaded Alg/Chit@$Mn_{0.8}Zn_{0.2}Fe_2O_4$ are shown in Fig. 3. The spectra indicate a wide peak of Chit at around 3447 cm^{-1} exhibiting vibration stretching of $-NH_2$ and $-OH$ groups. From the

Table I Zeta Potential, Polydispersity Index, and Hydrodynamic Size of Various Nanoparticle Formulations

Sample	Zeta potential (mV) ± SD	Particle size (nm) ± SD	Polydispersity
(Mn, Zn) Fe_2O_4*	−36.8 (±0.37)	66.5 (±7.51)	0.08
Chit-Cur@(Mn, Zn) Fe_2O_4	+46.5 (±0.20)	111.7 (±6.60)	0.10
Alg/Chit-Cur@(Mn,Zn) Fe_2O_4	−24.8 (±0.28)	122.4 (±4.10)	0.09

*This is the naked/bare or uncoated NP

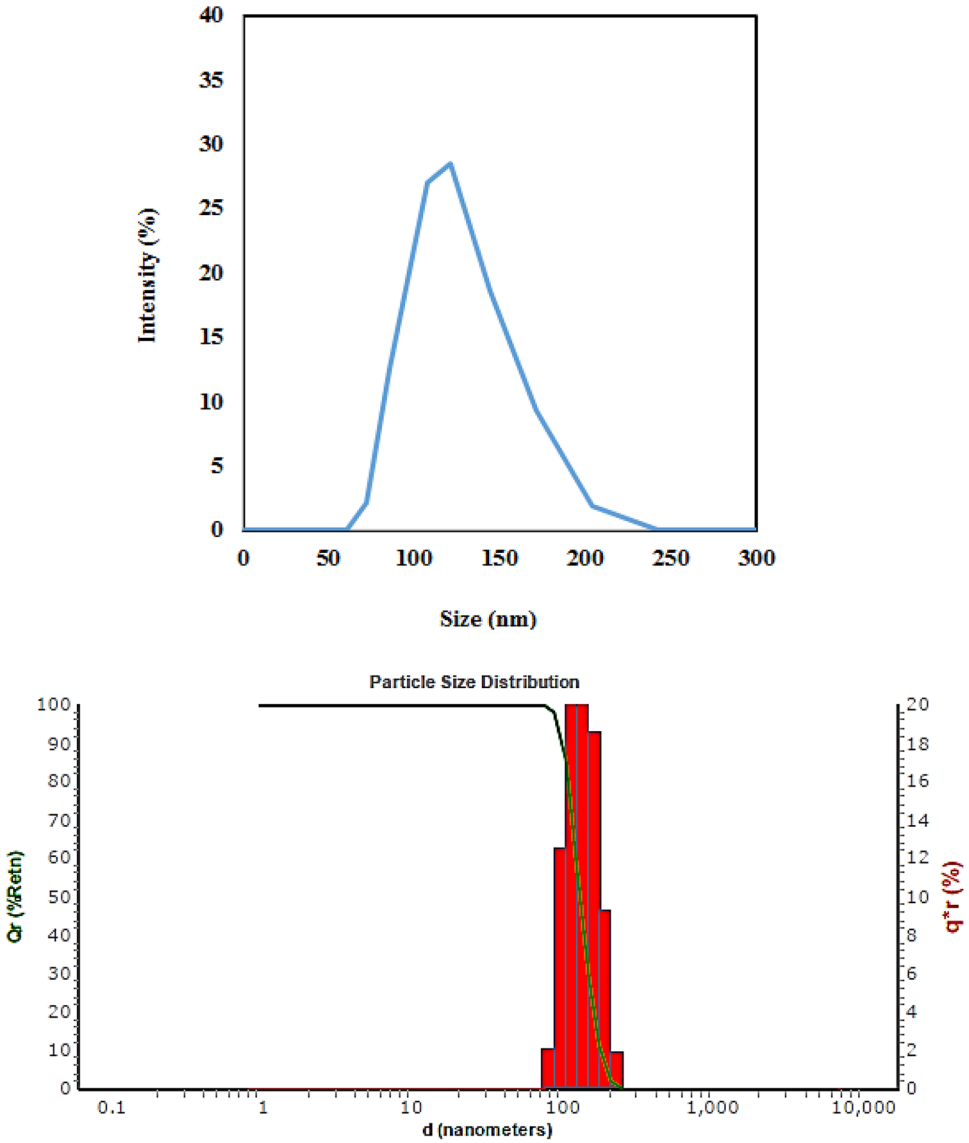

Fig. 1 DLS images of Alg/Chit/Cur@$Mn_{0.8}Zn_{0.2}Fe_2O_4$

Chit spectra, the peak around 1650 cm^{-1} was allocated to carbonyl vibration stretching. The peak around 1637 cm^{-1} on the Chit spectra was assigned to the N–H group.

The OH stretching of an Alg shows a peak at ~2891 cm^{-1}. The peak at ~1644 cm^{-1} was allocated to the carboxyl group. The C–O–C stretching of a saccharide shows a peak at ~2891 cm^{-1} and around 1127 cm^{-1}. In the Cur-loaded Alg/Chit@$Mn_{0.8}Zn_{0.2}Fe_2O_4$, the peak around 1649 cm^{-1} proves the presence of the carboxyl group of Alg overlapping with the NH group of Chit. Compared to Cur, in the Cur-loaded Alg/Chit@$Mn_{0.8}Zn_{0.2}Fe_2O_4$ spectra, there was a broad peak at ~3150–3486 cm^{-1} which indicated the addition of the OH group after the addition of Alg and Chit. In comparison with Chit, Alg, and Cur, the peak around 1640 cm^{-1} of Cur-loaded Alg/Chit@$Mn_{0.8}Zn_{0.2}Fe_2O_4$ assigned to the hydroxyl group overlapping with the NH_2 group of Chit [61]. Besides, in Cur-loaded Alg/Chit@$Mn_{0.8}Zn_{0.2}Fe_2O_4$, the band at approximately 590 cm^{-1} is due to the characteristic peaks of the Fe–O stretching vibrations of Fe_2O_4 [62]. Moreover, the observed peak at 460 cm^{-1} indicates Zn–O bonding [63]. The FTIR spectrum of Cur shows multiple peaks at 1508 cm^{-1} (C = C and C = O), 3478 cm^{-1} (N–H), and 1625 cm^{-1} (C = C). These peaks also appear in the FTIR spectrum of Cur-loaded NPs, but most of the peak intensities are relatively weak. These analyses suggest that Cur was effectively loaded into the particles [61].

XRD Analysis

Figure 4 illustrates the X-ray diffraction (XRD) patterns with different proportions of Mn:Zn in (Mn_x,Zn_{1-x}) Fe_2O_4 NPs with an x value in the range of 0.2 to 0.8. In the XRD pattern, all peaks at 2θ = 30.1°, 35°, 42°, 57°, and 62.25° can be ascribed to the diffraction of cubic (Mn,

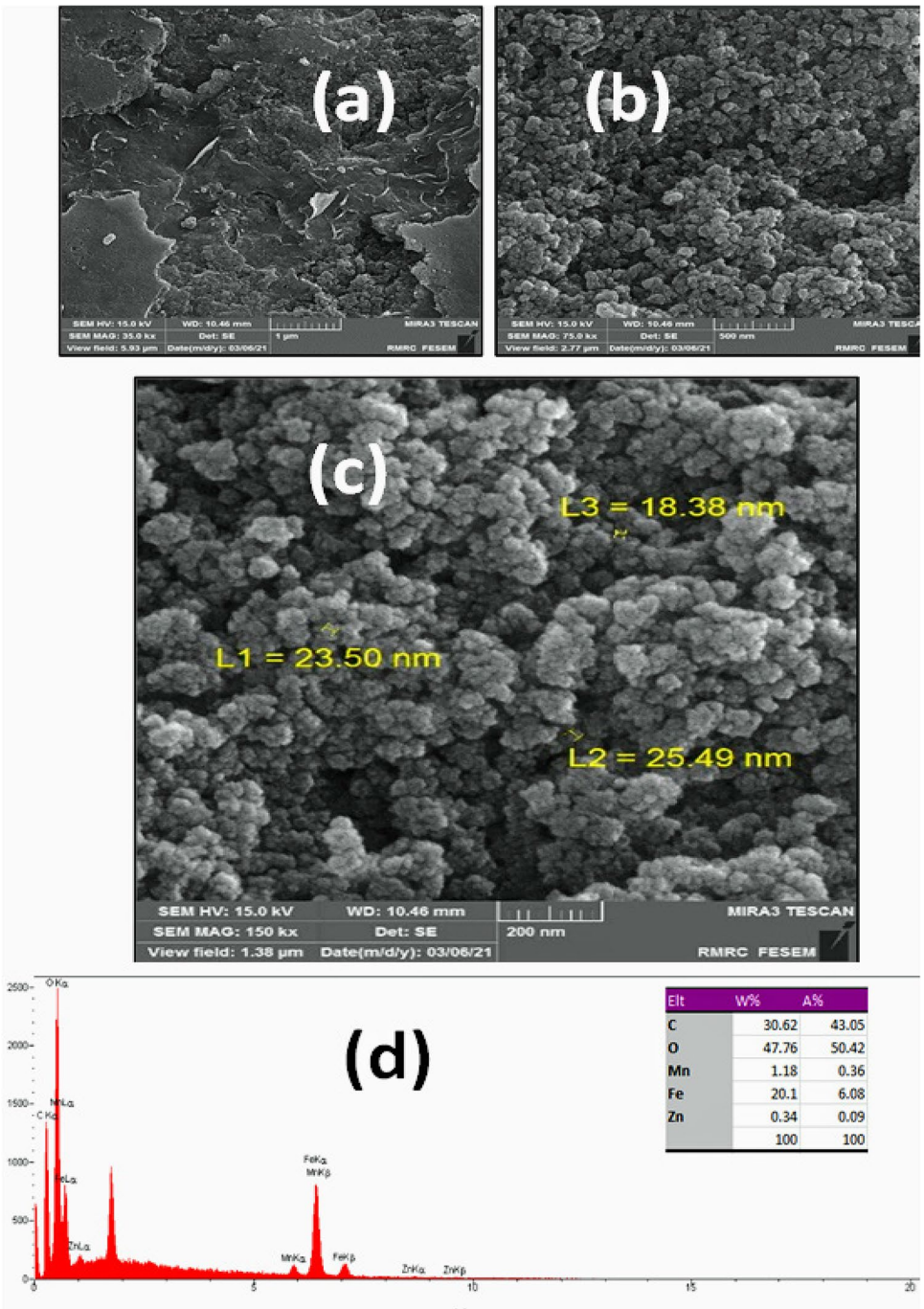

Fig. 2 **a** FE-SEM images of Alg/Chit/Cur@$Mn_{0.8}Zn_{0.2}Fe_2O_4$ with a magnification of ×35,000. **b** FE-SEM images of Alg/Chit/Cur@$Mn_{0.8}Zn_{0.2}Fe_2O_4$ with magnification of ×75,000. **c** FE-SEM images of Alg/Chit/Cur@$Mn_{0.8}Zn_{0.2}Fe_2O_4$ with a magnification of ×150,000. **d** EDX graph of Alg/Chit/Cur@$Mn_{0.8}Zn_{0.2}Fe_2O_4$. **e** Elemental map of Mn, Fe, C, O, Zn

Zn) ferrite crystal with the (220), (311), (400), (511), and (440) planes, respectively. All XRD diffractions display the characteristic peaks of the cubic structure, without any impurity of other metal oxides such as ZnO and MnO. It was also observed that the peaks in the XRD patterns were slightly shifted to lower angles with increasing Zn concentration. For instance, the situations of the (311) peaks are 35.55° for $Mn_{0.8}Zn_{0.2}Fe_2O_4$, 35.14° for $Mn_{0.6}Zn_{0.4}Fe_2O_4$, 34.75° for $Mn_{0.4}Zn_{0.6}Fe_2O_4$, and 34.7° for $Mn_{0.2}Zn_{0.8}Fe_2O_4$, respectively. The reduced angle of the diffraction peaks originating from the increased lattice spacing is in accordance with Bragg's law. Fe^{2+} ion and Mn^{2+} ion have a radius of 0.75 A° and 0.81 A°, respectively. This is smaller than the radius of a Zn^{2+} ion (0.88 A°), and therefore, the increase in Zn^{2+} ion substitution caused the expansion of the lattice spacing. This result confirms that the Mn^{2+} and Zn^{2+} ions were effectively doped in the relevant ferrite nanocrystals [64].

Fig. 2 (continued)

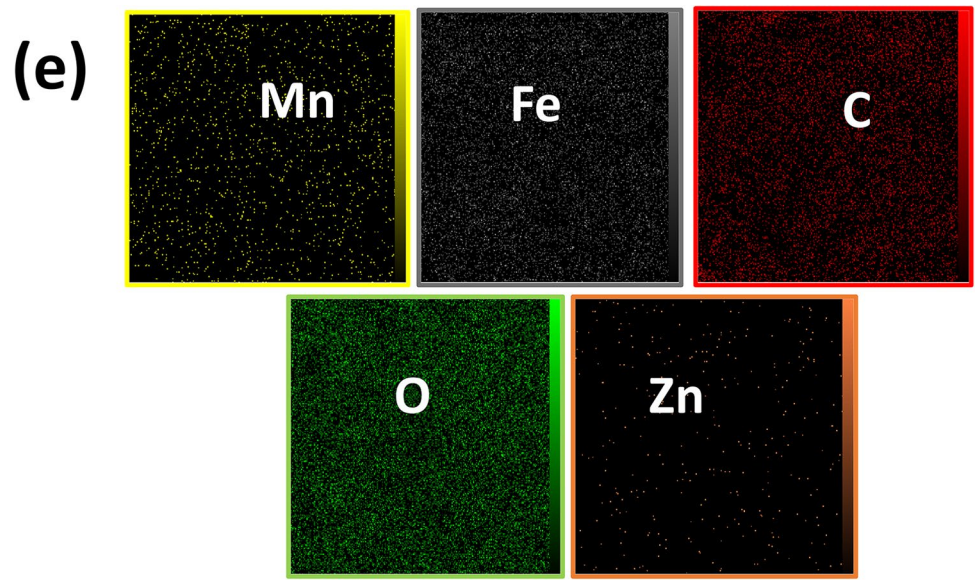

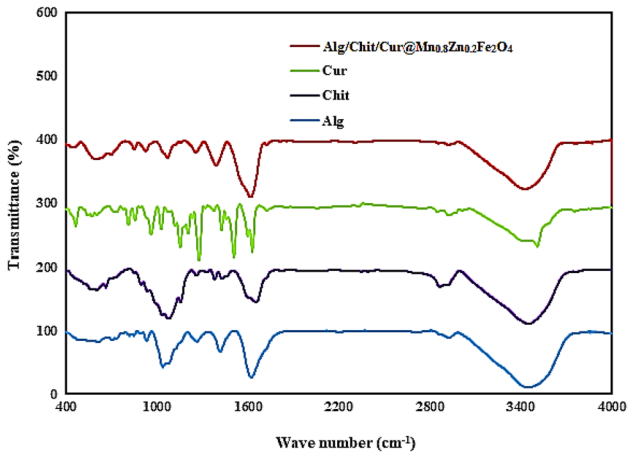

Fig. 3 FTIR spectra of Alg/Chit/Cur@$Mn_{0.8}Zn_{0.2}Fe_2O_4$, Cur, Chit, Alg

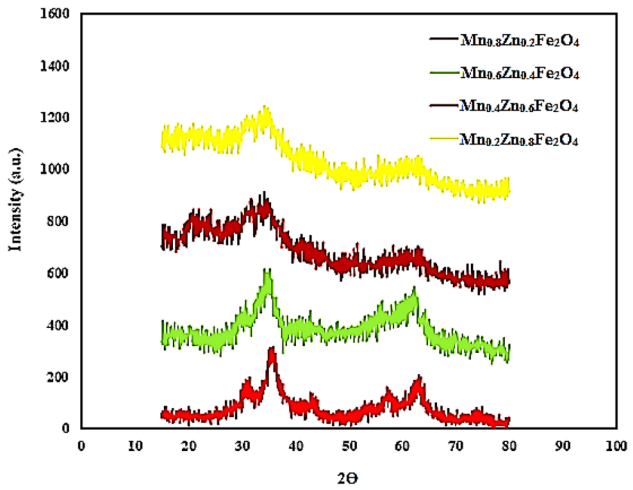

Fig. 4 XRD spectra of prepared magnetic $Mn_{1-x}Zn_xFe_2O_4$ MNPs

VSM Analysis

The magnetization curves of (Mn, Zn) ferrite with different ratios of (Mn:Zn) and Cur-loaded Alg/Chit@$Mn_{0.8}Zn_{0.2}Fe_2O_4$ are presented as Fig. 5. The hysteresis curves of the manufactured NPs do not display any coercivity magnetization. Nevertheless, all (Mn, Zn) ferrite nanoparticles show a saturation magnetization (MS), which indicates their paramagnetic behavior.

The MS of $Mn_{1-x}Zn_xFe_2O_4$ composite relied on the ratio of the Mn:Zn (Fig. 5a). The introduction of the Zn^{2+} dopants as non-magnetic ions in the nanostructure led to a decrease in MS. The variation in MS was caused by the effect of the occupancy of cations in specific sites and cationic stoichiometry. The presence of the polymer shell could reduce the MS of NPs in the latter NPs. The MS of $Mn_{0.8}Zn_{0.2}Fe_2O_4$ (34.6 emu/g) NP was higher than that of Cur-loaded Alg/Chit@$Mn_{0.8}Zn_{0.2}Fe_2O_4$ (23.9 emu/g) NPs (Fig. 5b). Even though the magnetization of the Cur-loaded Alg/Chit@$Mn_{0.8}Zn_{0.2}Fe_2O_4$ was less than that of the uncoated polymer, it still presented acceptable magnetic properties. Montha *et al*. prepared doxorubicin (DOX)-loaded PLGA@Chit@(Mn, Zn) ferrite NPs through the co-precipitation method and found the MS of the PLGA@Chit@$Mn_{0.9}Zn_{0.1}Fe_2O_4$ (13.2 emu/g) NPs to be lower than the $Mn_{0.9}Zn_{0.1}Fe_2O_4$ (56.1 emu/g) NPs due to the presence of the polymer shell in the latter NPs. Besides, at concentrations of less than 125 µg/mL, the DOX-PLGA@Chit@$Mn_{0.9}Zn_{0.1}$ferrite NPs exhibited lower toxicity against HeLa cells compared to the free DOX. At higher concentrations (e.g., 250 µg/mL), the DOX-PLGA@Chit@$Mn_{0.9}Zn_{0.1}$ ferrite revealed a relatively higher anti-cancer activity to HeLa cells compared to free DOX [65]. Li *et al*. reported that Mn–Zn ferrite inserted in a polymer matrix showed low Curie temperature close to

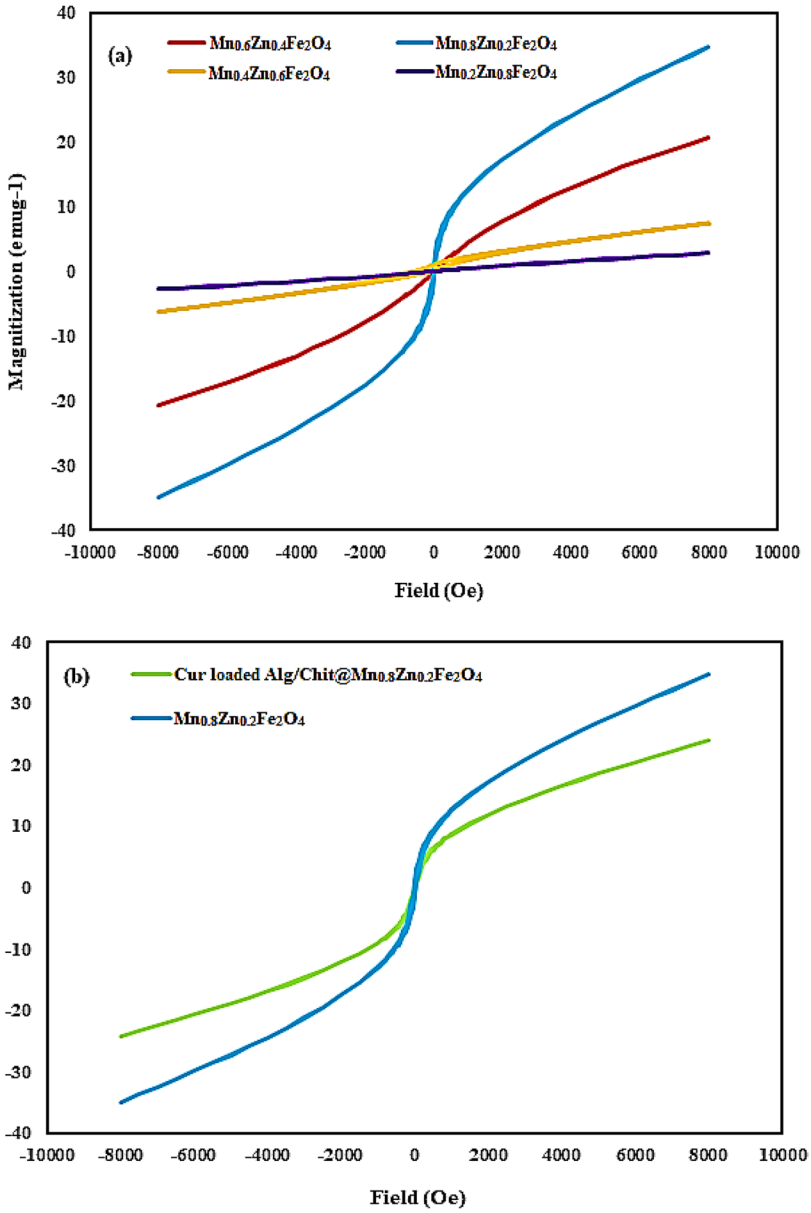

Fig. 5 **a** Magnetization curves of the $Mn_{1-x}Zn_xFe_2O_4$ MNPs. **b** Magnetization curves of the as-prepared Cur-loaded Alg/Chit@$Mn_{0.8}Zn_{0.2}Fe_2O_4$ and $Mn_{0.8}Zn_{0.2}Fe_2O_4$ NPs

the body temperature which was beneficial for safety and clinical viability [66].

In Vitro Release of Cur and Cur From Alg/Chit@ $Mn_{0.8}Zn_{0.2}Fe_2O_4$

The *in vitro* release study was assessed at pre-determined time intervals. The *in vitro* drug release study of Cur and Cur-loaded MNPs is depicted in Fig. 6. Pure Cur released around 5% of its drug load within 5 h followed by a 10% release at 36 h. To control the release rate, Alg beads are blended with Chit to prepare a complex through ion-ion, hydrogen bonding, and dipole-ion interactions [67, 68]. The release studies showed that 18% of Cur was released from the MNPs after 1 h. After 25 h, the release of curcumin increased slowly and finally reached 61% within 36 h. The initial release of Cur from Alg/Chit@$Mn_{0.8}Zn_{0.2}Fe_2O_4$ MNPs is attributed to the fraction of the drug which is adsorbed or weakly bound to the surface area of the Chit and the slow and controlled release of Cur is due to hydrogen bonding or Van der Waals forces between Cur and Chit [69]. In comparison with free Cur, the gradual increase in the release of Cur from Alg/Chit@$Mn_{0.8}Zn_{0.2}Fe_2O_4$ MNPs can be related to its uniform dispersibility and capability to keep the drug in a solubilized condition without causing precipitation. In fact, the natural polymers that covered the Cur during the preparation process may be responsible for the sustained release profile.

Zhao et al. developed layer-by-layer functionalized Fe_3O_4 nanoparticles by coating MNPs with positively

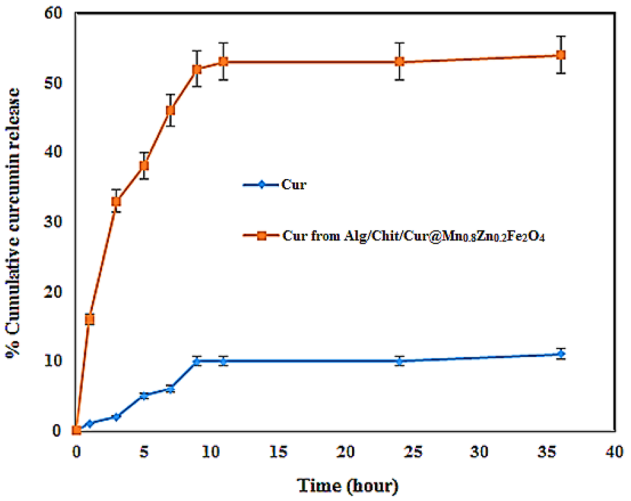

Fig. 6 Release of Cur and Cur from Alg/Chit/Cur@$Mn_{0.8}Zn_{0.2}Fe_2O_4$ MNPs

charged Chit and negatively charged Alg. Cur-loaded magnetic Alg/Chit nanoparticles were used to enhance the uptake efficiency, bioavailability, and cytotoxicity of Cur to Human Caucasian Breast Adenocarcinoma cells. The authors postulated that the release rate of Cur can be controlled by adding more layers of Chit and Alg as well as by changing the outermost polymer (Chit or Alg). An increase in the biopolymer layers caused a slower Cur release profile, whereas Chit as the outermost layer presented a faster Cur release [70]. Naderi *et al*. prepared magnetic $MnFe_2O_4$ and Fe_3O_4 MNPs with crosslinked carboxymethyl Chit hydrogel (CMCS). The maximum Cur release was obtained ranging 25.1–51.52% because of the weak bonds from the surface of Fe_3O_4/CMCS and $MnFe_2O_4$/CMCS [71].

MTT Assay

Cytotoxicity properties of Alg/Chit@$Mn_{0.8}Zn_{0.2}Fe_2O_4$, Cur, and Cur-loaded Alg/Chit@$Mn_{0.8}Zn_{0.2}Fe_2O_4$ MNPs were performed by using the MTT assay. This assay was performed at various concentrations (250, 125, 62.5, 31.25, and 15.625 µg/mL) of Alg/Chit@$Mn_{0.8}Zn_{0.2}Fe_2O_4$, Cur, and Cur-loaded Alg/Chit@$Mn_{0.8}Zn_{0.2}Fe_2O_4$ MNPs. Figure 7 indicates the effect of Alg/Chit@$Mn_{0.8}Zn_{0.2}Fe_2O_4$, Cur, and Cur-loaded Alg/Chit@$Mn_{0.8}Zn_{0.2}Fe_2O_4$ MNPs and chemotherapeutics on MCF-7 cells through the MTT assay after 48 h of exposure. Cur has the potential to operate through several pathways in cancer cells [72]. In comparison with the untreated cells ($p \leq 0.05$), the MTT outcomes showed that the growth of MCF-7 cells was meaningfully inhibited after the treatment with Cur-loaded synthesized NPs and Cur. The Cur-loaded Alg/Chit@$Mn_{0.8}Zn_{0.2}Fe_2O_4$ at a concentration of 250 µg/mL displayed the highest inhibition (81%) for the MCF-7 cells after 48 h of exposure. The effectiveness of Cur-loaded Alg/Chit@$Mn_{0.8}Zn_{0.2}Fe_2O_4$ MNPs on the MCF-7 cell line was considerably higher than the free Cur. The IC_{50} value of Cur-loaded Alg/Chit@$Mn_{0.8}Zn_{0.2}Fe_2O_4$ in MCF-7 cells was about 90.6 µg/mL, which is significantly lower than free Cur (213 µg/mL). It can therefore be proposed that the cytotoxicity of Cur-loaded Alg/Chit@$Mn_{0.8}Zn_{0.2}Fe_2O_4$ MNPs is because of the improvement of water solubility and internalization ability inferred on Cur as a result of the NP manufacturing process. Cur-loaded Alg/Chit@$Mn_{0.8}Zn_{0.2}Fe_2O_4$ MNPs and free Cur displayed a considerable impact on the cancer cells, which indicates that Cur

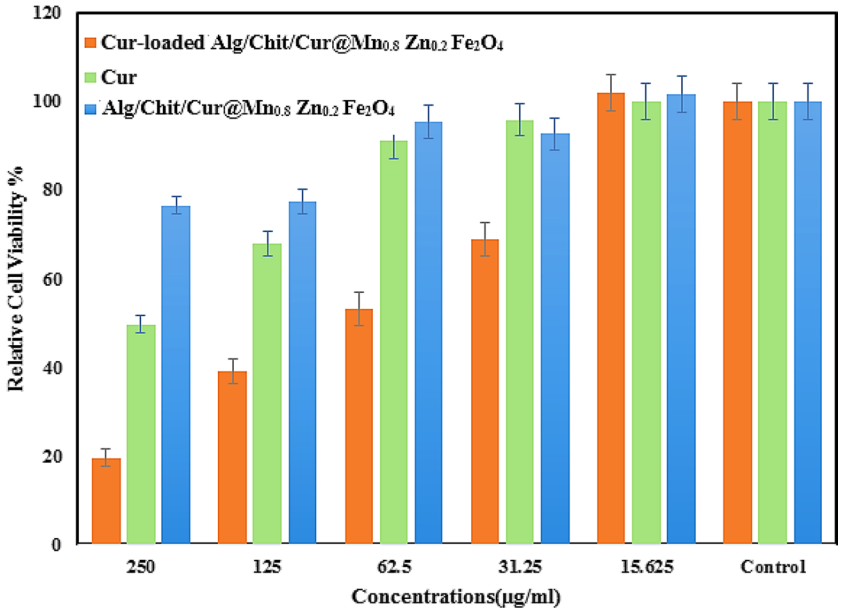

Fig. 7 Cell viability of breast cancer cells with different amounts of Cur-loaded Alg/Chit@$Mn_{0.8}Zn_{0.2}Fe_2O_4$, Cur, and Alg/Chit@$Mn_{0.8}Zn_{0.2}Fe_2O_4$ for 48 h determined by MTT assay

preserved its anti-tumor property even after encapsulation in Alg/Chit@$Mn_{0.8}Zn_{0.2}Fe_2O_4$ MNPs. No significant toxicity was detected on the cells related to the plain Alg/Chit@$Mn_{0.8}Zn_{0.2}Fe_2O_4$ MNPs, indicating the potential of Alg/Chit@$Mn_{0.8}Zn_{0.2}Fe_2O_4$ MNPs as a useful carrier for biomedical applications.

Conclusion

The formulation of Curcumin (Cur)-loaded alginate/chitosan@$Mn_{0.8}Zn_{0.2}Fe_2O_4$ MNPs exhibited highly promising therapeutic efficacy in combatting MCF-7 cancer cells. The nanoparticles underwent rigorous characterization through various techniques, including Fourier-transform infrared spectroscopy (FTIR), X-ray diffraction (XRD), and field emission scanning electron microscopy (FE-SEM). These analyses unveiled a magnetic core enveloped by a polymer shell, affirming the desired structural features and demonstrating a satisfactory degree of magnetic responsiveness. Notably, FE-SEM examinations revealed that the Cur-loaded alginate/chitosan@$Mn_{0.8}Zn_{0.2}Fe_2O_4$ MNPs possessed a mean particle size of approximately 20 nm. The *in vitro* biological testing showed a clear dose-dependent cytotoxic effect of the Cur-loaded NPs on MCF-7 cells. Importantly, this cytotoxicity surpassed that observed with free Cur, signifying the enhanced therapeutic potential of the nanomaterial formulation. Remarkably, the highest inhibition activity, amounting to an impressive 81%, was achieved at a concentration of 250 µg/mL of the Cur-loaded MNPs. One particularly intriguing discovery of importance that emerged from the investigations was that an ascending trend in the Mn content, transitioning from $x = 0.2$ to $x = 0.8$, resulted in a corresponding increase in the saturation magnetization of the $Mn_xZn_{1-x}Fe_2O_4$ NPs. These remarkable outcomes strongly indicate that Cur-loaded alginate/chitosan@$Mn_{0.8}Zn_{0.2}Fe_2O_4$ MNPs hold substantial promise as a desirable chemotherapy agent. it is therefore the belief of the authors that further investigation, particularly around *in vivo* studies, is warranted to unlock their full therapeutic potential and pave the way for potential clinical applications.

Author Contribution Fatemeh Ahmadi: writing—original draft, formal analysis, conceptualization; Majid Saeedi: supervision, investigation; Jafar Akbari: data curation, project administration; Mohammad Seyedabadi: validation; Pedram Ebrahimnejad: resources; Katayoun Morteza-Semnani: investigation; Monire Moalem-Banhangi: investigation, formal analysis; Amirhossein Babaei: formal analysis; Seyyed Mohammad Hassan Hashemi: formal analysis; Kofi Asare-Addo: writing—reviewing and editing; Ali Nokhodchi: supervision, writing—reviewing and editing; Shahram Ghasemi: investigation.

Funding This research was funded by Mazandaran University of Medical Sciences Research Council, Sari, Iran, grant number 8210.

Data Availability The data are available on request.

Declarations

Competing Interests The authors declare no competing interests.

References

1. Sahadevan J, Sojiya R, Padmanathan N, Kulathuraan K, Shalini M, Sivaprakash P, et al. Magnetic property of Fe_2O_3 and Fe_3O_4 nanoparticle prepared by solvothermal process. Mater Today: Proc. 2022;58:895–7.
2. Bustamante-Torres M, Romero-Fierro D, Estrella-Nuñez J, Arcentales-Vera B, Chichande-Proaño E, Bucio E. Polymeric composite of magnetite iron oxide nanoparticles and their application in biomedicine: a review. Polymers. 2022;14(4):752.
3. Pashchenko A, Liedienov N, Pashchenko V, Prokopenko V, Burhovetskii V, Voznyak A, et al. Modification of multifunctional properties of the magnetoresistive $La_{0.6}Sr_{0.15}Bi_{0.15}Mn_{1.1-x}B_xO_3$-δ ceramics when replacing manganese with 3d-ions of Cr, Fe Co, Ni. J Alloys Compd. 2018;767:1117–25.
4. Abdulvakhidov K, Ubushaeva E, Mardasova I, Vitchenko M, Abdulvakhidov B, Zaletov V, et al. Phase transitions, magnetic and dielectric properties of $PbFe_{0.5}Nb_{0.5}O_3$. Ferroelectrics. 2016;494(1):182–91.
5. Amirov AA, Chaudhari YA, Bendre ST, Chichay KA, Rodionova VV, Yusupov DM, et al. Phase transitions and magnetoelectric coupling in $BiFe_{1-x}Zn_xO_3$ multiferroics. Eur Phys J B. 2018;91:1–5.
6. Trukhanov A, Panina L, Trukhanov S, Kostishyn V, Turchenko V, Vinnik D, et al. Critical influence of different diamagnetic ions on electromagnetic properties of $BaFe_{12}O_{19}$. Ceram Int. 2018;44(12):13520–9.
7. Gambhir RP, Rohiwal SS, Tiwari AP. Multifunctional surface functionalized magnetic iron oxide nanoparticles for biomedical applications: a review. Appl Surf Sci Adv. 2022;11:100303.
8. Fatimah I, Fadillah G, Purwiandono G, Sahroni I, Purwaningsih D, Riantana H, et al. Magnetic-silica nanocomposites and the functionalized forms for environment and medical applications: a review. Inorg Chem Commun. 2022;137:109213.
9. Ansari MJ, Kadhim MM, Hussein BA, Lafta HA, Kianfar E. Synthesis and stability of magnetic nanoparticles. BioNanoScience. 2022;12(2):627–38.
10. Shokrollahi H. Magnetic properties and densification of manganese–zinc soft ferrites ($Mn1_{1-x}Zn_xFe_2O_4$) doped with low melting point oxides. J Magn Magn Mater. 2008;320(3–4):463–74.
11. Galinetto P, Albini B, Bini M, Mozzati MC. Chapter 11: Raman spectroscopy in zinc ferrites nanoparticles. In Do Nascimen GM, editor. Raman spectroscopy. Publisher InTech; 2018, p 223.

12. Liu XL, Wang YT, Ng CT, Wang R, Jing GY, Yi JB, et al. Coating engineering of $MnFe_2O_4$ nanoparticles with superhigh T2 relaxivity and efficient cellular uptake for highly sensitive magnetic resonance imaging. Adv Mater Interfaces. 2014;1(2):1300069.
13. Kim D-H, Nikles DE, Brazel CS. Synthesis and characterization of multifunctional chitosan-$MnFe_2O_4$ nanoparticles for magnetic hyperthermia and drug delivery. Materials. 2010;3(7):4051–65.
14. Deraz N, Alarifi A. Microstructure and magnetic studies of zinc ferrite nano-particles. Int J Electrochem Sci. 2012;7(7):6501–11.
15. Kącki M, Ryłko MS, Hayes JG, Sullivan CR. Measurement methods for high-frequency characterizations of permeability, permittivity, and core loss of Mn-Zn ferrite cores. IEEE Trans Power Electron. 2022;37(12):15152–62.
16. Mirbagheri M, Mirzaee O, Tajally M, Shokrollahi H. Synthesis, structure, hyperthermia behavior and magnetic properties of Mn–Zn particles prepared by a new method of ball-milling and heating. Physics Open. 2023;14:100139.
17. Shatti W, Abbas ZMA, Khodair Z. Co-precipitation method for the preparation of Mn-Zn ferrite and study their structural and magnetic properties. J Ovonic Res. 2022;18(4):473–9.
18. Aisida SO, Alnasir MH, Botha S, Bashir A, Bucher R, Ahmad I, et al. The role of polyethylene glycol on the microstructural, magnetic and specific absorption rate in thermoablation properties of Mn-Zn ferrite nanoparticles by sol–gel protocol. Eur Polym J. 2020;132:109739.
19. Zheng Z, Zhong X, Zhang Y, Yu H, Zeng D. Synthesis, structure and magnetic properties of nanocrystalline $Zn_xMn_{1-x}Fe_2O_4$ prepared by ball milling. J Alloys Compd. 2008;466(1–2):377–82.
20. Thakur A, Mathur P, Singh M. Study of dielectric behaviour of Mn–Zn nano ferrites. J Phys Chem Solids. 2007;68(3):378–81.
21. Hui BH, Salimi MN, editors. Production of iron oxide nanoparticles by co-precipitation method with optimization studies of processing temperature, pH and stirring rate. IOP Conference Series: Materials Science and Engineering; 2020: IOP Publishing.
22. Dhavale RP, Dhavale R, Sahoo S, Kollu P, Jadhav S, Patil P, et al. Chitosan coated magnetic nanoparticles as carriers of anticancer drug Telmisartan: pH-responsive controlled drug release and cytotoxicity studies. J Phys Chem Solids. 2021;148:109749.
23. Huang C-H, Chuang T-J, Ke C-J, Yao C-H. Doxorubicin–Gelatin/Fe_3O_4–alginate dual-layer magnetic nanoparticles as targeted anticancer drug delivery vehicles. Polymers. 2020;12(8):1747.
24. Cheraghali S, Dini G, Caligiuri I, Back M, Rizzolio F. PEG-coated MnZn ferrite nanoparticles with hierarchical structure as MRI contrast agent. Nanomaterials. 2023;13(3):452.
25. Zhang Q, Liu Q, Du M, Vermorken A, Cui Y, Zhang L, et al. Cetuximab and Doxorubicin loaded dextran-coated Fe_3O_4 magnetic nanoparticles as novel targeted nanocarriers for non-small cell lung cancer. J Magn Magn Mater. 2019;481:122–8.
26. Ebrahimnejad P, Nikookar SH, Fazeli-Dinan M, Payman Ziapour S, Farmoudeh A, Babaei A, et al. Preparation, characterisation and comparative toxicity of nanopermethrin against *Anopheles stephensi* and *Culex pipiens*. Trop Med Int Health. 2021;26(8):982–92.
27. Islam MM, Shahruzzaman M, Biswas S, Sakib MN, Rashid TU. Chitosan based bioactive materials in tissue engineering applications—a review. Bioact Mater. 2020;5(1):164–83.
28. Peng W, Li D, Dai K, Wang Y, Song P, Li H, et al. Recent progress of collagen, chitosan, alginate and other hydrogels in skin repair and wound dressing applications. Int J Biol Macromol. 2022;208:400–8.
29. Mahjoub MA, Ebrahimnejad P, Shahlaee F, Ebrahimi P, Sadeghi-Ghadi Z. Preparation and optimization of controlled release nanoparticles containing cefixime using central composite design: an attempt to enrich its antimicrobial activity. Curr Drug Deliv. 2022;19(3):369–78.
30. Li S, Zhang H, Chen K, Jin M, Vu SH, Jung S, et al. Application of chitosan/alginate nanoparticle in oral drug delivery systems: prospects and challenges. Drug Deliv. 2022;29(1):1142–9.
31. Nikolova D, Simeonov M, Tzachev C, Apostolov A, Christov L, Vassileva E. Polyelectrolyte complexes of chitosan and sodium alginate as a drug delivery system for diclofenac sodium. Polym Int. 2022;71(6):668–78.
32. Karim A, Rehman A, Feng J, Noreen A, Assadpour E, Kharazmi MS, et al. Alginate-based nanocarriers for the delivery and controlled-release of bioactive compounds. Adv Colloid Interface Sci. 2022;307:102744.
33. Ghosh D, Neog TT, Patra R, Nath K, Sarkar K. Alginate based scaffolds in tissue engineering and regenerative medicine. Alginate Biomaterial: Drug Delivery Strategies and Biomedical Engineering: Springer; 2023. p. 389-423.
34. Pontes-Quero GM, Benito-Garzón L, Cano JP, Aguilar MR, Vázquez-Lasa B. Amphiphilic polymeric nanoparticles encapsulating curcumin: antioxidant, anti-inflammatory and biocompatibility studies. Mater Sci Eng: C. 2021;121:111793.
35 Lal B. A review study on benefits of turmeric. ACADEMICIA: Int Multidiscip Res J. 2021;11(12):547–53.
36. Sharifi S, Fathi N, Memar MY, Hosseiniyan Khatibi SM, Khalilov R, Negahdari R, et al. Anti-microbial activity of curcumin nanoformulations: new trends and future perspectives. Phytother Res. 2020;34(8):1926–46.
37. Jahanbakhshi F, Dana PM, Badehnoosh B, Yousefi B, Mansournia MA, Jahanshahi M, et al. Curcumin anti-tumor effects on endometrial cancer with focus on its molecular targets. Cancer Cell Int. 2021;21(1):1–7.
38. Montazeri M, Sadeghizadeh M, Pilehvar-Soltanahmadi Y, Zarghami F, Khodi S, Mohaghegh M, et al. Dendrosomal curcumin nanoformulation modulate apoptosis-related genes and protein expression in hepatocarcinoma cell lines. Int J Pharm. 2016;509(1–2):244–54.
39. Lotfi-Attari J, Pilehvar-Soltanahmadi Y, Dadashpour M, Alipour S, Farajzadeh R, Javidfar S, et al. Co-delivery of curcumin and chrysin by polymeric nanoparticles inhibit synergistically growth and hTERT gene expression in human colorectal cancer cells. Nutr Cancer. 2017;69(8):1290–9.
40. Tavakoli F, Jahanban-Esfahlan R, Seidi K, Jabbari M, Behzadi R, Pilehvar-Soltanahmadi Y, et al. Effects of nano-encapsulated curcumin-chrysin on telomerase, MMPs and TIMPs gene expression in mouse B16F10 melanoma tumour model. Artif Cells Nanomedicine Biotechnol. 2018;46(sup2):75–86.
41. Prathyusha E, Prabakaran A, Ahmed H, Dethe MR, Agrawal M, Gangipangi V, et al. Investigation of ROS generating capacity of curcumin-loaded liposomes and its in vitro cytotoxicity on MCF-7 cell lines using photodynamic therapy. Photodiagnosis Photodynamic Ther. 2022;40:103091.
42. Yang X, Kuang Z, Yang X, Hu X, Luo P, Lai Q, et al. Facile synthesis of curcumin-containing poly (amidoamine) dendrimers as pH-responsive delivery system for osteoporosis treatment. Colloids Surf B: Biointerfaces. 2023;222:113029.
43. Kesharwani P, Johnston TP, Sahebkar A. Anticancer potential of curcumin-cyclodextrin complexes and their pharmacokinetic properties. Int J Pharm. 2022;631:122474.
44. Madamsetty VS, Vazifehdoost M, Alhashemi SH, Davoudi H, Zarrabi A, Dehshahri A, et al. Next-generation hydrogels as biomaterials for biomedical applications: exploring the role of curcumin. ACS Omega. 2023;8(10):8960–76.
45. Peng S, Li Z, Zou L, Liu W, Liu C, McClements DJ. Enhancement of curcumin bioavailability by encapsulation in sophorolipid-coated nanoparticles: an in vitro and in vivo study. J Agric Food Chem. 2018;66(6):1488–97.

46. Mukherjee S, Ray G, Gandhi P, Kar SK. Nano curcumin: making it useful for human therapy. J Nanomed Nanotechnol. 2020;11(487):1–10.
47. Saraswat A, Patki M, Fu Y, Barot S, Dukhande VV, Patel K. Nanoformulation of PROteolysis TArgeting Chimera targeting 'undruggable'c-Myc for the treatment of pancreatic cancer. Nanomedicine. 2020;15(18):1761–77.
48. Fu Y, Saraswat A, Wei Z, Agrawal MY, Dukhande VV, Reznik SE, et al. Development of dual ARV-825 and nintedanib-loaded PEGylated nano-liposomes for synergistic efficacy in vemurafnib-resistant melanoma. Pharmaceutics. 2021;13(7):1005.
49. Rezaeidian J, Naseh V, Entezari M, Hashemi M. Curcumin- and piperine-loaded Fe_3O_4@SiO_2 magnetic nanoparticles: synthesis, characterization, and comparison of the effects on MCF-7 breast cancer cell line. 2023; Posted on rd Feb:1-22 (preprint).
50. Omrani Z, Pourmadadi M, Yazdian F, Rashedi H. Preparation and characterization of pH-sensitive chitosan/starch/MoS_2 nanocomposite for control release of curcumin macromolecules drug delivery; application in the breast cancer treatment. Int J Biol Macromol. 2023;250:125897.
51. Saraswat AL, Maher TJ. Development and optimization of stealth liposomal system for enhanced in vitro cytotoxic effect of quercetin. J Drug Deliv Sci Technol. 2020;55:101477.
52. Zadeh ES, Ghanbari N, Salehi Z, Derakhti S, Amoabediny G, Akbari M, et al. Smart pH-responsive magnetic graphene quantum dots nanocarriers for anticancer drug delivery of curcumin. Mater Chem Phys. 2023;297:127336.
53. Patel A, Saraswat A, Patel H, Chen Z-S, Patel K. Palmitoyl carnitine-anchored nanoliposomes for neovasculature-specific delivery of gemcitabine elaidate to treat pancreatic cancer. Cancers. 2022;15(1):182.
54. Sadeghzadeh H, Pilehvar-Soltanahmadi Y, Akbarzadeh A, Dariushnejad H, Sanjarian F, Zarghami N. The effects of nanoencapsulated curcumin-Fe_3O_4 on proliferation and hTERT gene expression in lung cancer cells. Anti-Cancer Agents Med Chem (Formerly Current Medicinal Chemistry-Anti-Cancer Agents). 2017;17(10):1363-73.
55. Saraswat A, Vemana HP, Dukhande VV, Patel K. Galactose-decorated liver tumor-specific nanoliposomes incorporating selective BRD4-targeted PROTAC for hepatocellular carcinoma therapy. Heliyon. 2022;8(1):e08702.
56. Božič M, Elschner T, Tkaučič D, Bračič M, Hribernik S, Stana Kleinschek K, et al. Effect of different surface active polysaccharide derivatives on the formation of ethyl cellulose particles by the emulsion-solvent evaporation method. Cellulose. 2018;25(12):6901–22.
57. Khmara I, Strbak O, Zavisova V, Koneracka M, Kubovcikova M, Antal I, et al. Chitosan-stabilized iron oxide nanoparticles for magnetic resonance imaging. J Magn Magn Mater. 2019;474:319–25.
58. Nomani A, Nosrati H, Manjili HK, Khesalpour L, Danafar H. Preparation and characterization of copolymeric polymersomes for protein delivery. Drug Res. 2017;67(08):458–65.
59. Yang J, Fan L, Xu Y, Xia J. Iron oxide nanoparticles with different polymer coatings for photothermal therapy. J Nanoparticle Res. 2017;19(10):1–12.
60. Pazouki N, Irani S, Olov N, Atyabi SM, Bagheri-Khoulenjani S. Fe_3O_4 nanoparticles coated with carboxymethyl chitosan containing curcumin in combination with hyperthermia induced apoptosis in breast cancer cells. Prog Biomater. 2022;11(1):43–54.
61. Suryani, Halid NHA, Akib NI, Rahmanpiu, Mutmainnah N, editors. Preparation of curcumin nanoparticle by using reinforcement ionic gelation technique. AIP Conference Proceedings; 2017: AIP Publishing LLC.
62. Matli PR, Zhou X, Shiyu D, Huang Q. Fabrication, characterization, and magnetic behavior of porous $ZnFe_2O_4$ hollow microspheres. Int Nano Lett. 2015;5(1):53–9.
63. Tadjarodi A, Imani M, Salehi M. $ZnFe_2O_4$ nanoparticles and a clay encapsulated $ZnFe_2O_4$ nanocomposite: synthesis strategy, structural characteristics and the adsorption of dye pollutants in water. RSC Adv. 2015;5(69):56145–56.
64. Beji Z, Hanini A, Smiri L, Gavard J, Kacem K, Villain F, et al. Magnetic properties of Zn-substituted MnFe2O4 nanoparticles synthesized in polyol as potential heating agents for hyperthermia. Evaluation of their toxicity on Endothelial cells. Chem Mater. 2010;22(19):5420–9.
65. Montha W, Maneeprakorn W, Buatong N, Tang I-M, Pon-On W. Synthesis of doxorubicin-PLGA loaded chitosan stabilized (Mn, Zn) Fe_2O_4 nanoparticles: biological activity and pH-responsive drug release. Mater Sci Eng: C. 2016;59:235–40.
66. Li J, Qu Y, Ren J, Yuan W, Shi D. Magnetocaloric effect in magnetothermally-responsive nanocarriers for hyperthermia-triggered drug release. Nanotechnology. 2012;23(50):505706.
67. Jain S, Datta M. Montmorillonite-alginate microspheres as a delivery vehicle for oral extended release of venlafaxine hydrochloride. J Drug Deliv Sci Technol. 2016;33:149–56.
68. Bera H, Ippagunta SR, Kumar S, Vangala P. Core-shell alginate-ghatti gum modified montmorillonite composite matrices for stomach-specific flurbiprofen delivery. Mater Sci Eng: C. 2017;76:715–26.
69. Luo Z, Liu C, Quan P, Yang D, Zhao H, Wan X, et al. Mechanistic insights of the controlled release capacity of polar functional group in transdermal drug delivery system: the relationship of hydrogen bonding strength and controlled release capacity. Acta Pharm Sin B. 2020;10(5):928–45.
70. Song W, Su X, Gregory DA, Li W, Cai Z, Zhao X. Magnetic alginate/chitosan nanoparticles for targeted delivery of curcumin into human breast cancer cells. Nanomaterials. 2018;8(11):907.
71. Naderi Z, Azizian J. Synthesis and characterization of carboxymethyl chitosan/Fe_3O_4 and $MnFe_2O_4$ nanocomposites hydrogels for loading and release of curcumin. J Photochem Photobiol B: Biol. 2018;185:206–14.
72. Soren S, Jena SR, Samanta L, Parhi P. Antioxidant potential and toxicity study of the cerium oxide nanoparticles synthesized by microwave-mediated synthesis. Appl Biochem Biotechnol. 2015;177(1):148–61.